Available online at www.sciencedirect.com
ScienceDirect
Journal of Nuclear Materials 363–365 (2007) 994–999
journal of nuclear materials
www.elsevier.com/locate/jnucmat

The dynamics and structure of edge-localized-modes in Alcator C-Mod

J.L. Terry [a,*], I. Cziegler [a], A.E. Hubbard [a], J.A. Snipes [a], J.W. Hughes [a], M.J. Greenwald [a], B. LaBombard [a], Y. Lin [a], P. Phillips [b], S. Wukitch [a]

[a] *Plasma Science and Fusion Center, MIT, 175 Albany St., Cambridge, MA 02139, USA*
[b] *Fusion Research Center, University of Texas-Austin, Austin, TX 78712, USA*

Abstract

Characteristics of discrete ELMs produced in Alcator C-Mod discharges of low edge collisionality ($0.2 < \nu^* < 1$) and large lower triangularity ($\delta_{\text{lower}} \sim 0.75$) are examined. The energy lost per ELM from the H-mode pedestal is ~10% of the pedestal energy. These ELMs exhibit relatively long-lived precursor oscillations, often with two modes of intermediate toroidal mode number present. At the ELM 'crash' multiple plasma filament structures are expelled into the scrape-off-layer. A short-lived high frequency (~0.5 MHz) magnetic oscillation is initiated at the 'crash'. The initial ELM filaments are large perturbations to the SOL with radial extents of 0.5–1 cm and typical radial propagation velocities of 1 km/s. Velocities of up to 8 km/s have been seen. The poloidal extent of the initial filaments is >4.5 cm. The initial filaments are followed (at intervals of ~100 μs) by multiple, less perturbing secondary filaments.

PACS: 52.35.Py; 52.30.−q; 52.55.−s; 52.40.Hf

Keywords: Edge-localized-modes (ELMs); Cross-field transport; Edge transport; Alcator C-Mod; Visible imaging

1. Introduction

Edge-localized-modes (ELMs) are MHD instabilities that are typically responsible for periodically relaxing the steep pressure gradients at boundaries of tokamaks on a fast (~1 ms) time-scale. The steep edge-pressure gradients are responsible for the H-mode confinement regime. One of the serious consequences of ELMs is the large transient heat and particle load on the divertor plates. The problem is so serious that it threatens to limit the lifetime of these components in a burning plasma experiment like ITER [1]. Thus, the understanding and eventual mitigation of 'Type I' ELMs has been of intense interest to the magnetic-confinement-fusion community. While ELMs have been observed and studied for more than 20 years, new observations regarding their filamentary structure and complex dynamics have only recently emerged (see e.g. [2–5] and references therein). Characterizing and understanding the ELM phenomenon is also complicated by different manifestations or 'Types' of ELMs [6].

* Corresponding author. Fax: +1 617 253 0627.
E-mail address: terry@psfc.mit.edu (J.L. Terry).

0022-3115/$ - see front matter © 2007 Elsevier B.V. All rights reserved.
doi:10.1016/j.jnucmat.2007.01.266

On Alcator C-Mod ELMs are *not* the typical relaxation mechanism for the H-mode edge-pedestal, despite its often being close to the ballooning pressure limit. Enhanced-Dα (EDA) H-mode with the quasi-coherent mode [7] (QCM) is typical in C-Mod, although Type II ('grassy') ELMs [8] and larger Type III ELMs [9] are occasionally observed in some kinds of discharges. Recently an operational space has been accessed in C-Mod for which discrete, relatively large ELMs are the relaxation mechanism for the pedestal. This operational space is one of large triangularity for the lower half of the plasma ($\delta_{\rm lower} > 0.75$), small upper triangularity ($\delta_{\rm upper} \sim 0.15$), and a normalized collisionality in the pedestal $0.2 < \nu^* = \nu_{\rm ei}/\nu_{\rm bounce} < 1$ [10]. The plasma shape for producing these ELMs is shown in Fig. 1. These discharges can have high values for central $T_{\rm e}$ and $n_{\rm e}$ (reaching 4.5 keV and $2 \times 10^{20}\,{\rm m}^{-3}$ respectively) and good confinement, consistent with ITER98(y,2) ELMy H-mode scaling, i.e. $H_{\rm ITER98(y,2)} \sim 1$. The boundary with respect to $\delta_{\rm lower}$ appears to be quite sharp, since plasmas with $\delta_{\rm lower} = 0.72$ typically yield longer-lived 'dithers' between H- and L-mode, not ELMs. Plasmas with higher collisionalities typically exhibit EDA H-mode or EDA *and* small ELMs [10].

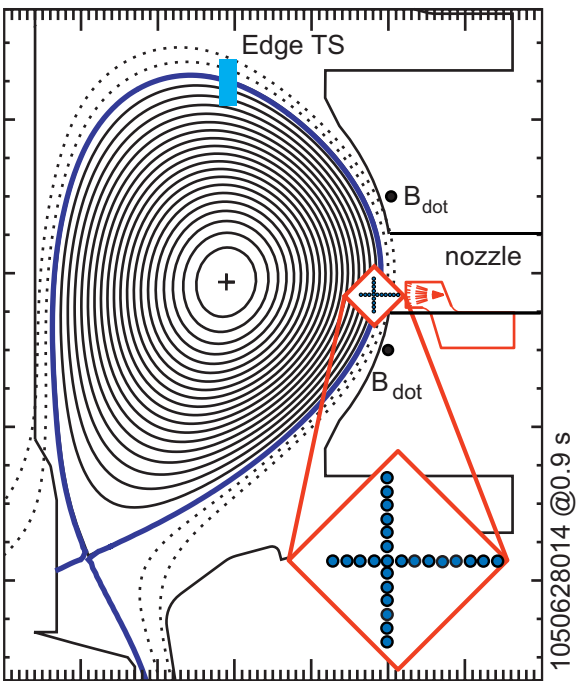

Fig. 1. The shaped C-Mod equilibrium for which the discrete ELMs are routinely obtained. Also shown is a schematic side view of the GPI optical arrays, the poloidal and radial locations of the limiter-mounted magnetic coils, and the location where the edge Thomson scattering measurements are made.

The 'Type' of these ELMs is, as yet, not clear. Nonetheless, as will be shown, (1) the $T_{\rm e}$ pedestal height can be ~900 eV (usually pedestals this hot are associated with Type I), (2) there is a precursor oscillation (typically present for Type III and sometimes for Type I), and (3) the pedestal, while reduced, is not completely destroyed during the ELM (the pedestal is sometimes destroyed by Type I).

There is a large body of literature on ELMs. Without attempting to review it, it is helpful to summarize what is known about those aspects that are specifically addressed in this paper. ELMs arise from instability to coupled peeling/ballooning modes of intermediate n, driven by pedestal pressure gradients and local (bootstrap) current [11]. Type III and sometimes Type I ELMs exhibit a precursor oscillation [12], evidence of this instability. Rapid growth to a non-linear phase ends in the expulsion of field-aligned filaments that carry heat and particles from the relatively hot pedestal to material surfaces of the device [2–5,13–18]. There are multiple filaments per ELM that are expelled at different times. The filaments propagate through the SOL with radial velocities that are typically <1 km/s [19–21,15].

The aspects of the discrete ELMs observed in these shaped C-Mod plasmas that will be reported here are: the effects of the ELM on the pedestal, the characteristics of the precursor, and the radial transport of the filaments. The primary diagnostics used for these characterizations are magnetic pickup coils mounted in two 'close-fitting' outboard limiters, two arrays of optical views looking at a toroidally localized D_2 gas puff (Gas-Puff-Imaging – GPI), and a Thomson scattering system with high spatial resolution at the plasma edge. The locations of these diagnostics in the poloidal plane are shown schematically in Fig. 1. There are 6 pairs of pickup coils; 3 pairs are separated toroidally in each of two outboard limiters. The optical diagnostic measures D_α emission from atoms supplied by puffing D_2 through a nozzle located close to the plasma edge. This local atom source results in toroidally localized emission that is viewed along tangential sightlines by in-vessel optics [22,23]. There are 2 optical arrays that view this local gas-puff, one is radial, with 15 views spanning the edge and SOL, while the other is vertical, with 12 views near the outboard mid-

plane, typically viewing just outside the separatrix. The gas puff nozzle is in the same poloidal plane as one pair of the limiter-mounted coils.

2. ELM energy losses

The energy lost from the plasma as a result of an ELM event has been studied extensively in other machines [13]. The ELMs studied here in C-Mod have only been produced in a limited operational space. For example, we have estimated the energy loss for only a limited range of densities, namely $n_e^{ped}/n_{greenwald} = 0.1$–$0.12$. Under these conditions, using the Thomson scattering system and ECE diagnostics, we find that ~10–20% of the pedestal's (electron) energy is lost during an ELM event. (Note that $\Delta W_{ELM}/W_{TOT} \lesssim 1\%$.) Nonetheless, the pedestal remains essentially intact during the ELM. These assertions are illustrated in Fig. 2, with 2(a) and (b) showing the pedestal profiles of temperature and density during an ELM, and with (c) showing the time history of the electron temperature in the middle of the pedestal, which is seen to drop by 10%, a drop similar to that seen for most of the ELMs studied. Estimates of the density loss during an ELM come from comparing 3 Thomson scattering profiles captured during an ELM (20–60 μs after the crash onset and before any significant pedestal recovery) with those captured before or after the same ELM. Scatter in the data and plasma changes allow us to bracket the density loss between 0% and 20%.

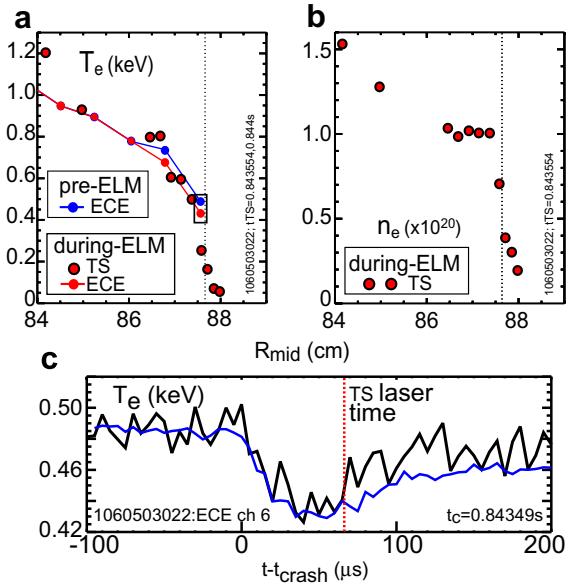

Fig. 2. (a) Profiles of edge T_e as measured by ECE (before (blue) and just after (red) an ELM crash), and by Thomson scattering (TS) just after the crash. (b) Profiles of edge density as measured by TS just after the crash. (c) Time history of T_e within the pedestal during the ELM for which the 'during-ELM' profiles were measured by TS. Also shown (blue) is the average T_e time history for 12 ELMs from the same discharge, normalized to the same pre-crash T_e. (For interpretation of the references to color in this figure legend, the reader is referred to the web version of this article.)

3. Structure and characteristics of the ELM precursor oscillation

The edge-localized-modes that give this phenomenon its name and precede the loss of particles and energy have also been studied extensively [12]. Precursors for ELMs observed in C-Mod during current ramp-up have been described previously in Ref. [9]. We will expand that description somewhat here. Some new aspects of the precursor are illustrated in Fig. 3. Fig. 3(a) shows the pre-crash oscillation (dB_θ/dt), as measured by one of the limiter-mounted magnetic pickup coils. There is frequently a relatively long (~100 μs) period of stable oscillation at 150–450 kHz. Similar to other machines, this precursor is of intermediate toroidal mode number $5 < n < 15$. There is often a clear beating in the oscillation, indicative of two main modes with $(f_1 + f_2)/2\Delta f \sim 10$. As shown in Fig. 3(b), f_1 and f_2 are 300 and 340 kHz in this case, probably indicative of modes with toroidal mode numbers differing by 1. Just before the ELM crash, the amplitude grows with a characteristic growth rate, $\gamma = 1$–$2 \times 10^5\ s^{-1}$, while the frequency drops to 50–100 kHz. Measurements of the phase at the 3 poloidal angles on the outboard side of the plasma yield an approximate local poloidal wavelength that is consistent with an approximately field-aligned mode, i.e. $\lambda_{pol} = (2\pi R_{ped} \tan\alpha)/n$, where α is the local field pitch and n is the toroidal mode number. For $n = 10$, $\lambda_{pol} = 10$ cm. The mode(s) rotate toroidally in the counter-current direction. Some resolution of the precursor in radial position is provided by the GPI radial array. The inside edge of the mode(s) extends beyond the innermost view, which is just inside the top of the pedestal ($\rho = R - R_{sep} \sim -10$ mm). Its outermost radial extent is inside the pedestal at $\rho \sim -5$ mm. Occasionally, the oscillation in the emission can be approximately π out of phase on the 2 pedestal views, implying a radial node between them. This is illustrated in Fig. 3(c).

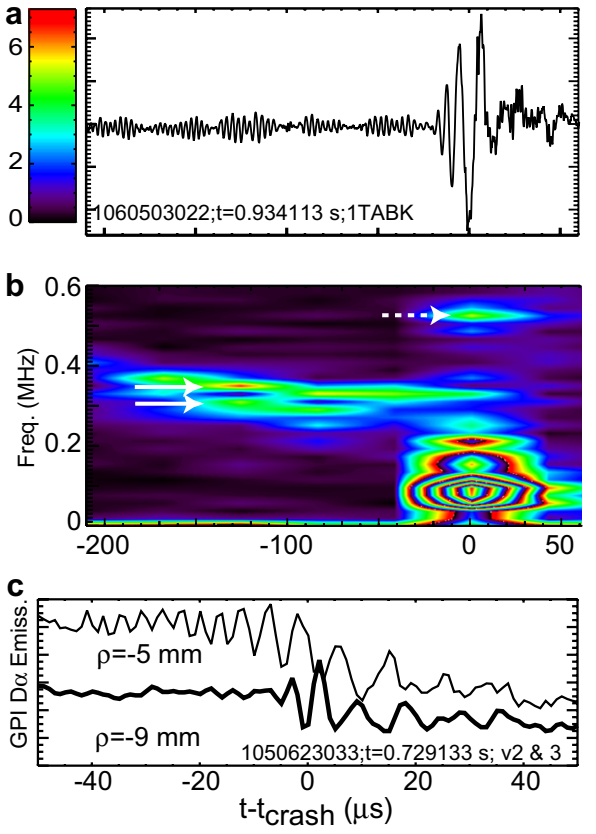

Fig. 3. (a) dB_θ/dt vs time during a typical ELM precursor oscillation and 'crash'. (b) The frequency spectrum of (a), showing the 2 mode frequencies responsible for the beating (solid arrows), the frequency downshift during the unstable growth (the amplitude color scale – shown at the left of (a) – wraps around for this feature), and the high frequency oscillation (dashed arrow) that begins at the time of the 'crash'. The spectrum has been smoothed both in time and frequency. (c) The GPI emission signals from adjacent views in the pedestal showing radial structure in the phase of the growing mode.

Also evident in Fig. 3(a) and (b) is the short burst of higher frequency activity ($f \sim 0.5$ MHz), starting at the time of the ELM 'crash', where the 'crash' time is defined as the instant when the pedestal T_e begins to drop. We speculate that it is involved with generation of the filaments.

4. ELM filament dynamics in the SOL

The GPI optical arrays also allow study of the dynamics of the ELM filaments as they propagate through the SOL. Within the 4.8 cm vertical coverage of the array we see multiple filaments per ELM event. The initial filament has the largest perturbation on the optical emission; hence we name it the 'primary'. The primary is typically followed by 2–5 'secondary' filaments (at least within the field-of-view of the arrays). The radial propagation of a primary and two secondary filaments is shown in Fig. 4. Typical radial widths for the primary are 0.5–1 cm. Radial propagation is quite rapid. As seen in the inset of Fig. 4, the distribution of radial speeds is peaked between 1 and 2 km/s. The secondary filaments are slower, 0.3–1 km/s, and some are seen to decelerate as they move out, e.g. the 2nd filament in Fig. 4. Their radial extent is in the same range as the primary filaments.

We do not resolve the poloidal extent of the filaments with the vertical optical array. We know that they are extended in the poloidal dimension, since 2D movies (300 frames taken at a 250 kHz frame rate) of the emission from the primary (imaged using GPI within the diamond shown in Fig. 1 – the same region that is viewed by the arrays) show

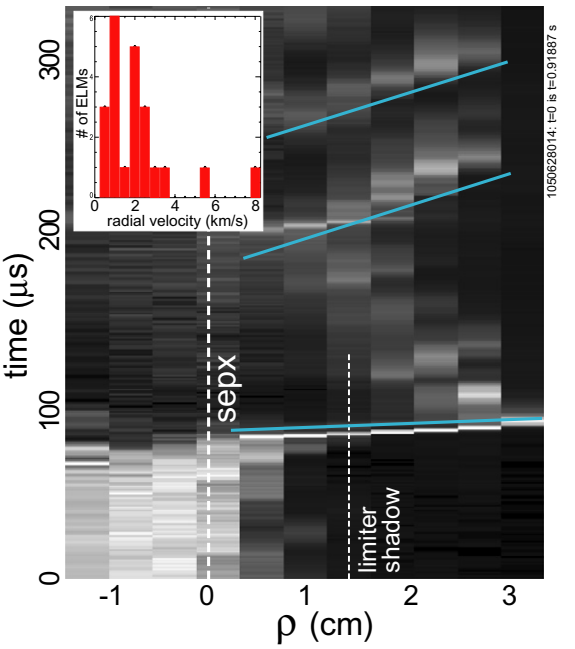

Fig. 4. GPI emission vs ρ (the distance into the SOL) and time from a single ELM. The time history of emission from each radial view is plotted vertically and normalized such that the maximum (minimum) emission in that view is white (black). Hence the views with $\rho < 0$ appear whiter before the crash, and the tilted straight lines that occur for views with $\rho < 0$ indicate the radial propagation of a primary ELM filament and 2 secondaries. Also evident is a feature occurring between the primary and the 1st secondary that appears to propagate inward. The cause of this feature is presently unknown. The distribution of the radial velocities of the 'primaries' is shown in the inset.

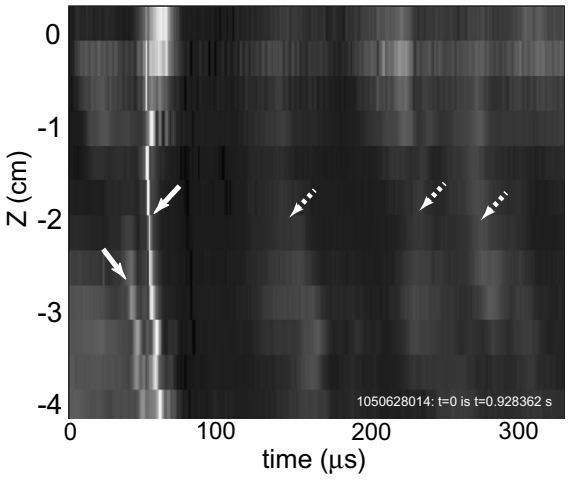

Fig. 5. GPI emission vs vertical position and time from a single ELM. (The position is relative to the midplane and the measurement is made at $\rho \sim 0.5$ cm.) 2 primaries (solid arrows) and 3 secondaries are seen.

them moving out as a sheet that essentially fills the vertical dimension of the imaged region, ~5 cm. This is consistent with what is seen when we plot the GPI emission time histories from the vertical array, as is done in Fig. 5, showing ELM filaments sweeping past the vertical array. Thus we interpret the slight 'tilt' in this and similar displays of filament propagation across the vertical array to be the result of a radially-thin, poloidally extended filament sheet peeling away from the plasma, rather than poloidal propagation of a poloidally-localized filament [16]. Its poloidal extent is larger than the 4.5 cm coverage of the array. In Fig. 5 *two* primaries (separated in time by only 13 μs) are seen; the upper portion of one appears on the lower part of the array, while the other fills all of the vertical views sequentially as it rapidly peels away. Observations of 'double' primaries like this are not uncommon. This means that we certainly do not observe all of the primary filaments in the limited coverage of the arrays and implies that there are more than the observed 2–5 secondary filaments occurring.

5. Discussion

Ultimately we desire to make a connection between these ELMs and the more typical pedestal relaxation manifestation in C-Mod, the QC mode of the EDA H-mode, believing that these relaxation 'types' (including the different ELM types) should be related. Thus we investigate the consequences of speculating that the QC mode could be a stabilized manifestation of the ELM precursor that occurs in pedestals of higher collisionality. There are some qualitative similarities. The QC mode frequency is typically ~250 kHz before being Doppler downshifted into the 60–150 kHz range by the co-current spin-up of the EDA H-mode discharge [24]. It propagates in the same (counter-current) direction as the precursor modes. We measure $\lambda_\theta = 2\pi/k_\theta$ of the QC mode to be ~6 cm at the outboard midplane [25], in roughly the same range as the poloidal wavelength of the ELM precursor. It also has a strong magnetic component [26]. Of course without additional theoretical and modeling investigation, this remains qualitative speculation.

We have characterized some aspects of the ELM filaments and their dynamics in the SOL. One difference between C-Mod filaments and those on most other tokamaks may be the radial propagation speed of the filaments. For example, the following radial speeds have been reported: ~0.45 km/s on 'average' [19], but up to 1–2 km/s [16] for 'primaries' in JET, between 1 and 2.4 km/s in JT60-U [20], $\lesssim$0.5 km/s in DIII-D (although with some ejections at nearly 7 km/s) [21], $\lesssim$1 km/s in MAST [18]. In C-Mod we observe a distribution peaked at 1 km/s, with some radial speeds as high as 8 km/s. With the exception of JT60-U and JET, the speeds on C-Mod are larger by factors of ~2. Inter-machine comparisons can be exploited for a better understanding of ELM dynamics.

Acknowledgement

This work is supported by DoE Coop. Agreement DE-FC02-99-ER54512 and Grant DE-FG03-96ER54373.

References

[1] ITER Physics Expert Group on Disruptions, Plasma Control, and MHD and ITER Physics Basis Editors, Nucl. Fus. 39 (1999) 2251.
[2] D.L. Rudakov, J.A. Boedo, R.A. Moyer, et al., Plasma Phys. Control. Fus. 44 (2002) 717.
[3] T. Eich, A. Herrmann, J. Neuhauser, Phys. Rev. Lett. 91 (2003) 195003.
[4] A. Kirk, H.R. Wilson, G.F. Counsell, et al., Phys. Rev. Lett. 92 (2004) 245002.
[5] A.W. Leonard, N. Asakura, J.A. Boedo, et al., Plasma Phys. Control. Fus. 48 (2006) A149.
[6] H. Zohm, Plasma Phys. Control. Fus. 38 (1996) 105.
[7] M. Greenwald, R. Boivin, P. Bonoli, et al., Phys. Plasmas 6 (1999) 1943.

[8] D.A. Mossessian, P. Snyder, A. Hubbard, et al., Phys. Plasmas 10 (2003) 1720.
[9] J.A. Snipes, A.E. Hubbard, D.T. Garnier, et al., Plasma Phys. Control. Fus. 38 (1996) 1127.
[10] A.E. Hubbard, K. Kamiya, N. Oyama, et al., Plasma Phys. Control. Fus. 48 (2006) A121.
[11] P.B. Snyder, H.R. Wilson, J.R. Ferron, et al., Phys. Plasmas 9 (2002) 2037.
[12] T. Kass, S. Guenter, M. Maraschek, et al., Nucl. Fus. 38 (1998) 111.
[13] A.W. Leonard, T.H. Osborne, M.E. Fenstermacher, et al., Phys. Plasmas 10 (2003) 1765.
[14] A. Kirk, G.F. Counsell, H.R. Wilson, et al., Plasma Phys. Control. Fus. 46 (2004) 551.
[15] T. Eich, A. Herrmann, G. Pautasso, et al., J. Nucl. Mater. 337–339 (2005) 669.
[16] M. Endler, I. Garcia-Cortes, C. Hidalgo, et al., Plasma Phys. Control. Fus. 47 (2005) 219.
[17] A. Kirk, T. Eich, A. Herrmann, et al., Plasma Phys. Control. Fus. 47 (2005) 995.
[18] A. Kirk, H.R. Wilson, R. Akers, et al., Plasma Phys. Control. Fus. 47 (2005) 315.
[19] W. Fundamenski, W. Sailer, Plasma Phys. Control. Fus. 46 (2004) 233.
[20] N. Asakura, M. Takechi, N. Oyama, T. Nakano, J. Nucl. Mater. 337–339 (2005) 712.
[21] J.A. Boedo, D.L. Rudakov, E.M. Hollmann, et al., J. Nucl. Mater. 337–339 (2005) 771.
[22] S.J. Zweben, D.P. Stotler, J.L. Terry, et al., Phys. Plasmas 9 (2002) 1981.
[23] J.L. Terry, S.J. Zweben, K. Hallatschek, et al., Phys. Plasmas 10 (2003) 1739.
[24] A. Mazurenko, M. Porkolab, D. Mossessian, et al., Phys. Rev. Lett. 89 (2002) 225004.
[25] J.L. Terry, N.P. Basse, I. Cziegler, et al., Nucl. Fus. 45 (2005) 1321.
[26] J.A. Snipes, B. LaBombard, M. Greenwald, et al., Plasma Phys. Control. Fus. 43 (2001) L23.